Supplementary Information for Monolayer MoS_2 Strained to 1.3% with a Microelectromechanical System

Jason W. Christopher, *Member, IEEE,* Mounika Vutukuru, David Lloyd, J. Scott Bunch, Bennett B. Goldberg, David J. Bishop, *Member, IEEE,* and Anna K. Swan *Senior Member, IEEE,*

S1. Tri-Layer Graphene Raman Analysis of Strain

The data presented in [1] shows complete slipping and no strain. Garza *et al.* found for their trilayer graphene sample that the G phonon peak shifted at a rate of -0.24 $cm^{-1}/\%$. We compare this shift rate with the expected rate given the literature values for the Grüneisen parameter and shear deformation potential for trilayer graphene (γ_G = 1.89 $\pm$ .02, and β_G = 0.71 $\pm$ .06) [2], the Poisson's ratio, ν, for Graphite (0.165) [3], and the fact that under strain the G peak shifts according to the same formula as the E' peak in MoS_2,

$$\omega_G^{\pm} = \omega_{0G}\left\{1 - \left[\gamma_G\left(1-\nu\right) \mp \frac{\beta_G}{2}\left(1+\nu\right)\right]\epsilon\right\}, \tag{S1}$$

where ω_{0G} is the unstrained phonon energy (1584.9) [1], and ϵ is the uniaxial strain. According to the given parameter values and the G phonon energy dependence on strain, it is expected that $\frac{d\omega_G^+}{d\epsilon} \approx -12$ $cm^{-1}/\%$ and $\frac{d\omega_G^-}{d\epsilon} \approx -38$ $cm^{-1}/\%$. This shows that the shift rate reported by Garza *et al.* is two orders of magnitude smaller than expected based on the literature. Such a large discrepancy strongly indicates that Garza *et al.* did not achieve the claimed strain.

We hypothesize that the graphene is completely slipping and the observed changes to the G peak position are the result of heating the sample. If proper error bars had been reported for the G peak position and Si Raman peak position used to determine sample temperature, then would be able to assess the likelihood of of our hypothesis. Without this information we can still strongly justify our hypothesis. Given the scattering of the G peak position measurements in Fig. 5a of [1] we think it is likely that a best fit linear regression would reveal that the G peak shifted by only ≈-1.5 cm^{-1} in their experiment. Assuming the G peak in trilayer graphene shifts with temperature by -0.015 $cm^{-1}/°C$, a conservative value considering the corresponding shift rates for monolayer and bilayer graphene [4], then the flake's temperature would have to increase by 100°C to explain the observations. This is about an 84°C greater temperature change than reported by Garza *et al.*. Using -0.0232 $cm^{-1}/°C$ as the Stokes parameter for poly-silicon as is done in Garza *et al.*, a 84°C change in temperature would be explained by a 1.9 cm^{-1} shift in the Si Raman peak. While this may seem like a large error, we find in our experience that the Si Raman peak in our poly-silicon structures can vary easily by as much as 0.4 cm^{-1} from location to location because of doping and internal strain inhomogeneities. Considering we see this much variation in our devices produced by a professional foundry, we do not think it is unreasonable that five times the variation could be seen in the home built devices in [1]. Further, our hypothesis matches the observed reproducibility, and nicely explains why the intensity of G and 2D peaks decrease so much when the actuator is operating at high power, reduced radiative decay because of thermally increased non-radiative decay channels. Lastly, note that when the actuators are operated at 2.4 W a 5 mm by 5 mm silicon wafer 625 μm thick would heat at a rate of 94°C/s without a heat sink. Hence, it is entirely possible that the device in [1] was not thermally grounded well enough and the temperature of the entire MEMS die rose by 100°C, which would bypass the protective measures used by Garza *et al.* to prevent thermally heating the flake.

During the preparation of this manuscript the authors became aware of a novel experiment using electron diffraction to measure strain in carbon nanotubes strained with MEMS [5]. As the field of strain based nano-material devices matures we

Manuscript received Mon. Day, Year. This work was supported by the National Science Foundation Division of Materials Research under grant number 1411008. DJB is supported by the Engineering Research Centers Program of the National Science Foundation under NSF Cooperative Agreement No. EEC-1647837.

J. W. Christopher is with the Department of Physics, Boston University, Boston, MA 02215.

M. Vutukuru is with the Department of Electrical and Computer Engineering, Boston University, Boston, MA 02215 USA.

D. Lloyd is with the Department of Mechanical Engineering, Boston University, Boston, MA 02215 USA.

J. S. Bunch is with the Department of Mechanical Engineering, Boston University, Boston, MA 02215 USA.

B. B. Goldberg is with the Department of Physics, Boston University, Boston, MA 02215 USA, and also with the Department of Physics and the Searle Center for Advancing Learning and Teaching, Northwestern University, Evanston, IL 60208 USA.

D. J. Bishop is with the Department of Electrical and Computer Engineering and Department of Physics, Boston University, Boston, MA 02215 USA.

A. K. Swan is with the Department of Electrical and Computer Engineering, Boston University, Boston, MA 02215 USA e-mail: swan@bu.edu

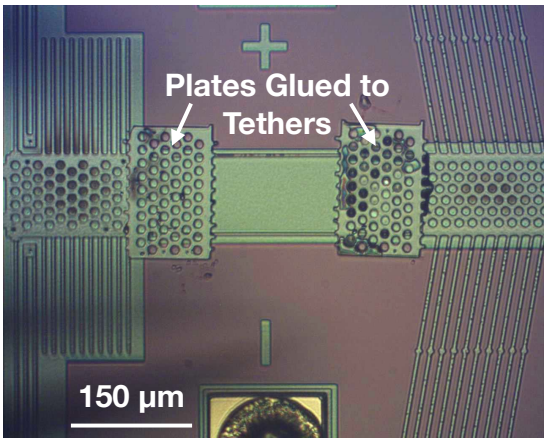

Fig. S1. Device M26 with shuttles from other devices glued onto the thermal relief tethers repairing them.

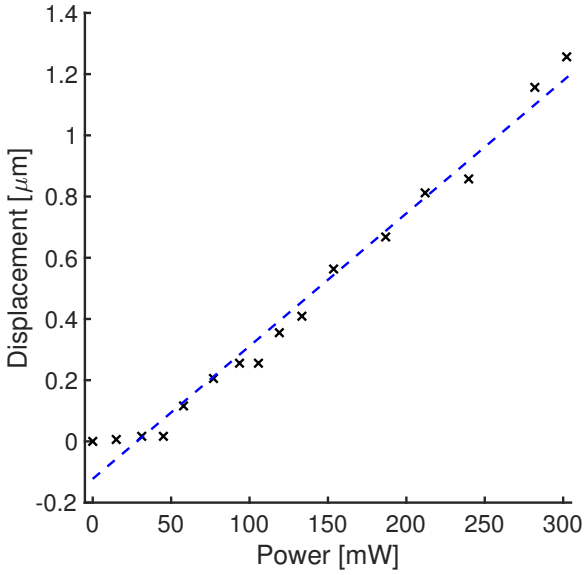

Fig. S2. Example shuttle displacement versus power applied curve for one of our thermal actuators.

believe electron diffraction for measuring strain is likely to become an important tool to irrefutably determine strain and offer important diagnostic capabilities in designing new strain based devices.

S2. Repair of Device M26

Fig. S1 shows device M26 repaired after the thermal relief tethers broke during its first actuation. The repair was accomplished by breaking free shuttles from discarded devices using probe tips in a micromanipulator. Then a micro-pipette system was used to dispense several micron-meter wide drops of UV curable glue, Norland Optical Adhesive NOA81, onto each shuttle. The holes in the shuttles acted like a sponge to wick up the glue. The shuttles were then carefully picked up and placed onto device M26 with a pair of probe tips actuated by micromanipulators. The device was then exposed to 20 seconds of UV radiation using Xenon Corp. RC-250B pulsed UV Curing System, solidifying the glue.

S3. Displacement vs. Power Curve

Fig. S2 shows an example optical measurement of displacement versus power applied to one of our thermal actuators. The slope is 4.3 nm/mW, which we used to estimate the rate at which we applied strain to our samples. For example if we had a sample with a 3 μm gap, our nominal gap size, and we wanted to increase the strain in steps of 0.2%, then we would increase the power in steps of $\approx$1.4 mW.

S4. Effective Poisson's Ratio

The equations for mechanical equilibrium of a coupled bulk and 2D system are derived below starting with the free energy equations for the bulk and 2D system, and coupling them using Lagrange multipliers. The total free energy is

$$H = \int_{\Sigma_B} \mathrm{d}V F_B\left(\epsilon^B\right) + \tau \int_{\Sigma_S} \mathrm{d}S \left[F_S\left(\epsilon^S\right) + \lambda_{ij}\left(\epsilon^B_{ij}\big|_{z=0} - \epsilon^S_{ij}\right)\right] \tag{S2}$$

where F_B, ϵ^B and F_S, ϵ^S are the free energy densities and strain tensors of the bulk material and surface (2D system), τ is the effective thickness of the 2D material, Σ_B is the volume of the bulk material, Σ_S is the surface of the 2D system, and λ_{ij} are Lagrange multipliers to constrain the strain of the 2D material and the bulk at the boundary, $z = 0$, to be equal. Since ϵ is symmetric, so too must λ otherwise there would be too many constraints. Summation over repeated induces is assumed. Note that ϵ^B is a three dimensional tensor, while ϵ^S is only a two dimensional tensor and only has support over the domain $z = 0$.

Now we can take functional derivatives with respect to the displacement fields u^B and u^S, bulk and surface, to determine the equilibrium equations and boundary conditions. We'll also define the stress tensor $\sigma_{ij}^X := \frac{\partial F_X}{\partial \epsilon_{ij}^X}$ where X can be B or S.

$$\begin{aligned}
\frac{\delta H}{\delta u_i^B} &= \int_{\Sigma_B} \mathrm{d}V \sigma_{jk}^B \frac{1}{2}\left(\delta_{ik}\partial_j \delta^{(3)}(x) + \delta_{ij}\partial_k \delta^{(3)}(x)\right) \\
&\quad + \tau \int_{\Sigma_S} \mathrm{d}S \lambda_{jk} \frac{1}{2}\left[\delta_{ik}\partial_j \delta^{(2)}(x) + \delta_{ij}\partial_k \delta^{(2)}(x)\right]\delta(z) && \text{(S3)} \\
&= \int_{\Sigma_B} \mathrm{d}V \left[\partial_j\left(\sigma_{ij}^B \delta^{(3)}(x)\right) - \delta^{(3)}(x)\,\partial_j \sigma_{ij}^B\right] \\
&\quad + \delta(z)\,\tau \int_{\Sigma_S} \mathrm{d}S \left[\partial_j\left(\lambda_{ij}\delta^{(2)}(x)\right) - \delta^{(2)}(x)\,\partial_j \lambda_{ij}\right] && \text{(S4)} \\
&= -\int_{\Sigma_B} \mathrm{d}V \delta^{(3)}(x)\,\partial_j \sigma_{ij}^B + \oint_{\partial\Sigma_B} \mathrm{d}A_j \sigma_{ij}^B \delta^{(3)}(x) \\
&\quad - \delta(z)\,\tau \int_{\Sigma_S} \mathrm{d}S\, \delta^{(2)}(x)\,\partial_j \lambda_{ij} + \delta(z)\,\tau \oint_{\partial\Sigma_S} \mathrm{d}\ell_j \lambda_{ij}\delta^{(2)}(x) && \text{(S5)} \\
&= -\int_{\Sigma_B} \mathrm{d}V \partial_j \sigma_{ij}^B \delta^{(3)}(x) + \int_{\partial\Sigma_B, z\neq 0} \mathrm{d}A_j \sigma_{ij}^B \delta^{(3)}(x) \\
&\quad + \delta(z) \int_{\Sigma_S = \partial\Sigma_B, z=0} \mathrm{d}S \left[\sigma_{ij}^B \hat{A}_j - \tau \partial_j \lambda_{ij}\right]\delta^{(2)}(x) \\
&\quad + \delta(z)\,\tau \oint_{\partial\Sigma_S} \mathrm{d}\ell_j \lambda_{ij}\delta^{(2)}(x) = 0, && \text{(S6)}
\end{aligned}$$

where $\delta^{(n)}$ is the n-dimensional Kronecker delta function, and $\partial\Sigma_X$ is used to denote the boundary of Σ_X. In the first line the partial derivative with respect to ϵ_{jk}^B is taken, and then the functional derivative of ϵ_{jk}^B. In the second line the sums are collapsed making use of the symmetry of ϵ and λ, and the first step of integration by parts, $f\partial_j g = \partial_j(fg) - g\partial_j f$, is used. In the third line the generalized Stoke's theorem is used to convert integrals over Σ_B and Σ_S to their boundaries, $\partial\Sigma_B$ and $\partial\Sigma_S$. The integration measures $\mathrm{d}A_j$ and $\mathrm{d}\ell_j$ are oriented outward of the integration domain. In the fourth line the portion of the integral over $\partial\Sigma_B$ that corresponds with Σ_S, *i.e.* where $z = 0$, is combined with the explicit integral over Σ_S. Setting each integrand equal to zero we arrive at the equilibrium conditions and boundary conditions for the bulk material.

$$\partial_j \sigma_{ij}^B = 0 \tag{S7}$$

$$\sigma_{ij}^B \hat{A}_j\Big|_{\partial\Sigma_B, z\neq 0} = 0 \tag{S8}$$

$$\sigma_{ij}^B \hat{A}_j\Big|_{z=0} - \tau\partial_j \lambda_{ij} = 0 \tag{S9}$$

$$\lambda_{ij}\hat{\ell}_j\Big|_{\partial\Sigma_S} = 0 \tag{S10}$$

Note that $\hat{A}_j$ and $\hat{\ell}_j$ are outward normal unit vectors of their domains. The first equation is the standard equilibrium equation for a bulk elastic material, and the second equation is the standard boundary condition for no external forces acting on the material. The third equation gives a rule for balancing the forces between the bulk material and the 2D system, and the fourth provides a no force boundary condition on the 2D system.

Now we determine the equilibrium equations and boundary conditions of the 2D system by taking the functional derivative with respect the the 2D system's displacement field.

$$\begin{aligned}
\frac{\delta H}{\delta u_i^S} &= \tau \int_{\Sigma_S} \mathrm{d}S \left(\sigma_{ij}^S - \lambda_{ij}\right)\partial_j \delta^{(2)}(x) && \text{(S11)} \\
&= \tau \int_{\Sigma_S} \mathrm{d}S \left\{\partial_j\left[\left(\sigma_{ij}^S - \lambda_{ij}\right)\delta^{(2)}(x)\right] - \delta^{(2)}(x)\,\partial_j\left(\sigma_{ij}^S - \lambda_{ij}\right)\right\} && \text{(S12)} \\
&= \tau\left\{\oint_{\partial\Sigma_S} \mathrm{d}\ell_j \left(\sigma_{ij}^S - \lambda_{ij}\right)\delta^{(2)}(x) - \int_{\Sigma_S} \mathrm{d}S\left[\partial_j\left(\sigma_{ij}^S - \lambda_{ij}\right)\delta^{(2)}(x)\right]\right\} = 0 && \text{(S13)}
\end{aligned}$$

This derivation followed the same exact steps as for $\frac{\delta H}{\delta u_i^B}$, but there are fewer terms and there is no complication of the boundary of one domain being part of another integrals domain. Setting each integrand equal to zero we have

$$\left(\sigma_{ij}^S - \lambda_{ij}\right)\hat{\ell}_j\Big|_{\partial\Sigma_S} = 0 \tag{S14}$$

$$\partial_j\left(\sigma_{ij}^S - \lambda_{ij}\right) = 0. \tag{S15}$$

We can now easily eliminate the Lagrange multipliers yielding the following set of equations

$$0 = \partial_j \sigma^B_{ij}, \tag{S16}$$

$$0 = \sigma^B_{ij} \hat{A}_j \Big|_{\partial\Sigma_B, z\neq 0}, \tag{S17}$$

$$0 = \sigma^B_{ij} \hat{A}_j \Big|_{z=0} - \tau \partial_j \sigma^S_{ij}, \tag{S18}$$

$$0 = \sigma^S_{ij} \hat{\ell}_j \Big|_{\partial\Sigma_S} \tag{S19}$$

$$0 = \epsilon^B_{ij}\big|_{z=0} - \epsilon^S_{ij}. \tag{S20}$$

As mentioned earlier the first two equations are the standard equilibrium equation and zero force boundary conditions of a bulk material. The third term relates the boundary force of the bulk to the interior force on the 2D material. Note that when $i = z$, the second term is zero. Further, for a system where the 2D material is at the $z = 0$ plane, $\hat{A}_j = \hat{z}$, so this equation reads $0 = \sigma^B_{iz}\big|_{z=0} - \tau\partial_j\sigma^S_{ij}$. The fourth equation is the standard no force boundary condition, but this time for a 2D system. The final equation is a reminder that though we have eliminated the Langrange multipliers, we still need to adhere to the constraints they impose. This is very important because otherwise you might think that you could decouple the bulk from the 2D system by creating a uniform strain distribution with zero off diagonal strain components, which would trivially satisfy Equation S18.

We'd really like to solve these equations in the situation of uniaxial strain in isotropic bulk and 2D materials. In the bulk situation this is solved by hypothesizing a uniform strain distribution, which trivially satisfies the equilibrium equation, and then solving for the strain components that satisfy the no force boundary conditions. If we tried to use the same method to solve these coupled equations it isn't hard to see that we will fail to satisfy the requirement that strains between the bulk and 2D system are equal. In short we'd find

$$\epsilon^B_{xy} = \epsilon^B_{xz} = \epsilon^B_{yz} = 0, \tag{S21}$$

$$\epsilon^B_{xx} = \epsilon, \quad \epsilon^B_{yy} = \epsilon^B_{zz} = -\nu_B \epsilon, \tag{S22}$$

$$\epsilon^S_{xy} = 0, \tag{S23}$$

$$\epsilon^S_{xx} = \epsilon, \quad \epsilon^S_{yy} = -\nu_S \epsilon, \tag{S24}$$

where ϵ is the stain along the x axis (major strain axis), and ν_B and ν_S are the Poisson's ratios of the bulk and 2D system. Unless $\nu_B = \nu_S$ these strains do not satisfy the requirement of Equation S20. There simply isn't a uniform solution to the coupled bulk, 2D material equations.

However, we can find a uniform strain field that does not violate the coupled equations so egregiously. Let's begin with what we want to respect most, Equation S18, and hypothesize that $\epsilon^B_{xx} = \epsilon^S_{xx} = \epsilon$ and $\epsilon^B_{yy} = \epsilon^S_{yy} = -\nu_{\text{eff}}\epsilon$. Now we try to satisfy as many boundary conditions as possible. Very easily we'll find $\epsilon^B_{xz} = \epsilon^B_{yz} = \epsilon^B_{xy} = \epsilon^S_{xy} = 0$. Setting $\sigma^B_{zz} = 0$ we'll find that $\epsilon^B_{zz} = -\nu_B \frac{1-\nu_{\text{eff}}}{1-\nu_B}\epsilon$. The remaining boundary conditions are $\sigma^B_{yy} = 0$ and $\sigma^S_{yy} = 0$. We could choose ν_{eff} to satisfy one of these, but that would mean setting ν_{eff} equal to ν_B or ν_S. Instead we choose to satisfy neither, and let energy minimization select the best ν_{eff}. Integrating the free energy density over the thickness of the bulk we find

$$\begin{aligned}\int \mathrm{d}z F_B\left(\epsilon^B\right) + \tau_S F_S\left(\epsilon^S\right) &= \frac{\tau_B}{2}\left(\sigma^B_{xx}\epsilon^B_{xx} + \sigma^B_{yy}\epsilon^B_{yy} + \sigma^B_{zz}\epsilon^B_{zz}\right) \\ &\quad + \frac{\tau_S}{2}\left(\sigma^S_{xx}\epsilon^S_{xx} + \sigma^S_{yy}\epsilon^S_{yy}\right) \qquad \text{(S25)} \\ &= \frac{\epsilon^2}{2}\sum_{X\in\{B,S\}} \frac{\tau_X E_X}{(1+\nu_X)(1-\nu_X)}\left(1 - 2\nu_X\nu_{\text{eff}} + \nu^2_{\text{eff}}\right) \qquad \text{(S26)}\end{aligned}$$

where τ_B and τ_S and E_B and E_S are the thicknesses and Young moduli of the bulk and 2D material. Let $\mathcal{K}_X := \frac{\tau_X E_X}{(1+\nu_X)(1-\nu_X)}$, then we can simply set the derivative with respect to ν_{eff} to zero in order to minimize the energy density. The solution is

$$\nu_{\text{eff}} = \frac{\mathcal{K}_B\nu_B + \mathcal{K}_S\nu_S}{\mathcal{K}_B + \mathcal{K}_S}. \tag{S27}$$

This solution has a nice intuitive balance. If the product of the thickness and the Young's modulus of the 2D material is small compared with the substrate, then the effective Poisson's ratio is that of the substrate. This is the typical assumption for 2D materials on bulk substrates. However, when the product of the thickness and the Young's modulus of the 2D material is large compared with the substrate, then the effective Poisson's ratio is that of the 2D material. In particular, if there isn't a substrate, $\mathcal{K}_B = 0$, we recover what we'd expect, $\nu_{\text{eff}} = \nu_S$.

TABLE S1
MAXIMUM CHANGE IN STRAIN ACHIEVED AND PRE-STRAIN

	Max. Change in Strain [%]			Pre-Strain [%]		
Device	$\nu = 0.42$	$\nu = 0.35$	$\nu = 0.27$	$\nu = 0.42$	$\nu = 0.35$	$\nu = 0.27$
M24	0.76 ± 0.08	0.72 ± 0.08	0.68 ± 0.08	-0.01 ± 0.09	-0.01 ± 0.05	-0.01 ± 0.05
M25	0.63 ± 0.05	0.59 ± 0.05	0.56 ± 0.05	-0.05 ± 0.03	-0.05 ± 0.03	-0.05 ± 0.03
M26	0.86 ± 0.11	0.82 ± 0.11	0.77 ± 0.10	0.03 ± 0.06	0.03 ± 0.06	0.02 ± 0.05
M26 v2	1.30 ± 0.09	1.23 ± 0.08	1.15 ± 0.08	-0.03 ± 0.03	-0.03 ± 0.03	-0.02 ± 0.03

TABLE S2
SLOPES FOR RAMAN PEAK STRAIN RESPONSE

	E'_- [cm^{-1}/%]			A' [cm^{-1}/%]		
Device	$\nu = 0.42$	$\nu = 0.35$	$\nu = 0.27$	$\nu = 0.42$	$\nu = 0.35$	$\nu = 0.27$
M24	-1.95 ± 0.12	-2.08 ± 0.14	-2.22 ± 0.13	-0.78 ± 0.68	-0.83 ± 0.71	-0.90 ± 0.68
M25	-2.28 ± 0.43	-2.41 ± 0.47	-2.56 ± 0.50	-0.73 ± 0.52	-0.78 ± 0.66	-0.83 ± 0.77
M26	-1.45 ± 0.49	-1.52 ± 0.50	-1.60 ± 0.48	-0.75 ± 0.57	-0.79 ± 0.65	-0.84 ± 0.75
M26 v2	-2.11 ± 0.19	-2.24 ± 0.21	-2.40 ± 0.20	-0.75 ± 0.46	-0.79 ± 0.42	-0.85 ± 0.44
Lit.	-2.32 ± 0.41	-2.45 ± 0.40	-2.60 ± 0.38	-0.49 ± 0.17	-0.55 ± 0.19	-0.62 ± 0.21

TABLE S3
SLOPES FOR PL PEAK STRAIN RESPONSE

	Trion [meV/%]			A Ex. [meV/%]			B Ex. [meV/%]		
Device	$\nu = 0.42$	$\nu = 0.35$	$\nu = 0.27$	$\nu = 0.42$	$\nu = 0.35$	$\nu = 0.27$	$\nu = 0.42$	$\nu = 0.35$	$\nu = 0.27$
M24	-55 ± 5	-59 ± 5	-63 ± 5	-45 ± 9	-48 ± 8	-52 ± 9	-71 ± 13	-76 ± 14	-81 ± 14
M25	-84 ± 12	-89 ± 13	-95 ± 14	-81 ± 20	-86 ± 25	-91 ± 21	-29 ± 14	-31 ± 15	-33 ± 17
M26	-110 ± 22	-116 ± 22	-124 ± 22	-72 ± 25	-76 ± 32	-80 ± 30	-74 ± 21	-78 ± 31	-82 ± 36
M26 v2	-43 ± 2	-46 ± 2	-49 ± 2	-38 ± 3	-40 pm 3	-43 ± 3	-50 ± 5	-53 ± 5	-57 ± 6
Lit.	-			-30 ± 2	-33 ± 2	-37 ± 3	-		

TABLE S4
RELATIVE SHIFT RATES OF PEAKS

					Literature		
Slope Ratio	M24	M25	M26	M26 v2	$\nu = 0.42$	$\nu = 0.35$	$\nu = 0.27$
$\frac{d\omega_{A'}}{dE_A}$ [cm^{-1}/eV]	18 ± 6	10 ± 3	8 ± 3	20 ± 5	17 ± 22	17 ± 22	17 ± 22
$\frac{dE_A}{d\omega_{E'}}$ [meV/cm^{-1}]	23 ± 3	36 ± 5	40 ± 8	18 ± 1	15 ± 6	15 ± 6	16 ± 6
$\frac{d\omega_{A'}}{d\omega_{E'}}$ [-]	.41 ± .15	.32 ± .12	.43 ± .17	.35 ± .10	.24 ± .34	.26 ± .35	.27 ± .37

S5. RESULTS ASSUMING DIFFERENT POISSON'S RATIO

To assess the possibility that the effective Poisson's ratio for our samples is different from that of PPC, 0.42, we re-calculated our results assuming a Poisson's ratio of 0.35 and 0.27. The results for all three values of the Poisson's ratio are tabulated in Table S1, Table S2, Table S3, and Table S4. These tables consistently show that our experiment is relatively insensitive to the Poisson's ratio, but there is a slightly better agreement between our experiment and literature as the Poisson's ratio decreases.

S6. STRESS AND STRAIN INHOMOGENEITY

To asses the inhomogeneity of stress and strain in our samples we simulated our experiment using COMSOL. Fig. S3 shows the resulting distributions of the stress and strain in our samples accounting for the expected trapezoidal shape. To accentuate the inhomogeneity we ran our simulations with 33% strain, and they still show a large region in the middle with highly uniform stress and strain. The simulation assumes a sample thickness of 0.65 nm, 32 μm wide on its widest side, 3 μm long, a Young's modulus of 270 GPa, and Poisson's ratio of 0.42. These simulations show the robustness of the strain homogeneity in the middle of the sample to perturbations at the edges, which is where inhomogeneities in the PPC and flake are most likely to occur.

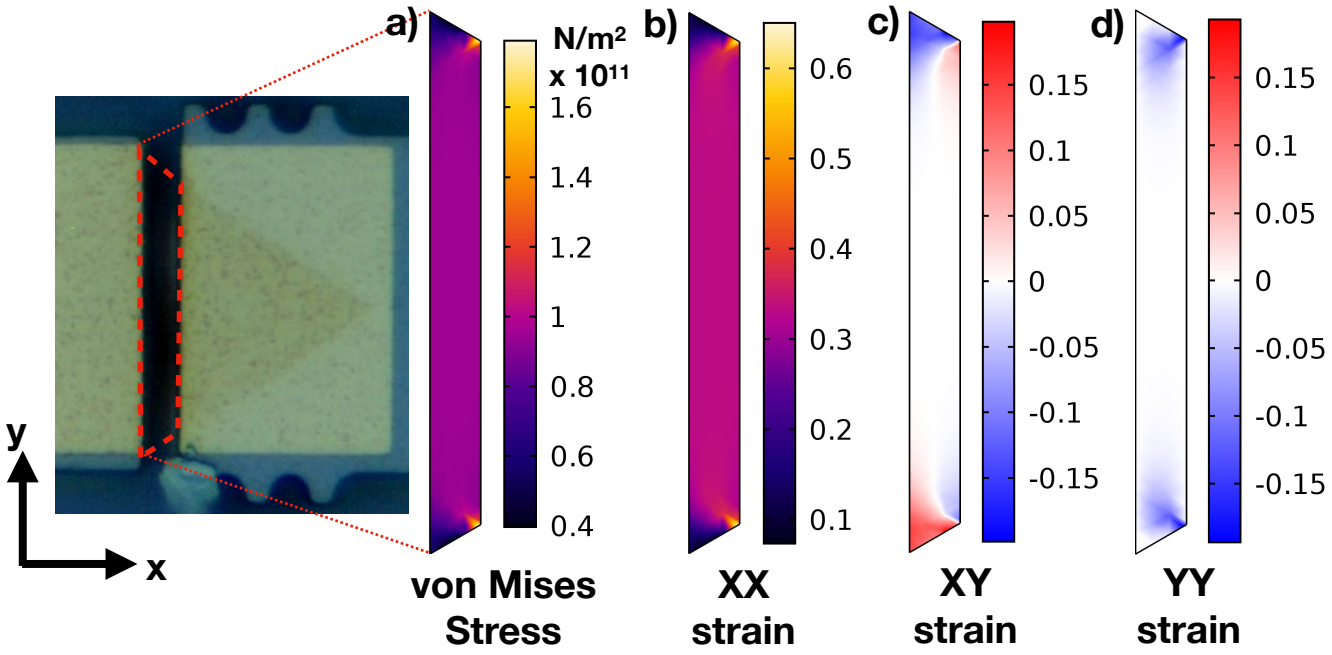

Fig. S3. Stress and Strain Homogeneity: a) von Mises Stress, b) XX component of the strain tensor, c) XY component of the strain tensor, d) YY component of the strain tensor

REFERENCES

[1] H. H. Perez Garza, E. W. Kievit, G. F. Schneider, and U. Staufer, "Controlled, reversible, and nondestructive generation of uniaxial extreme strains (>10%) in graphene," *Nano Letters*, vol. 14, no. 7, pp. 4107–4113, 2014.

[2] A. L. Kitt, Z. Qi, S. Rémi, H. S. Park, A. K. Swan, and B. B. Goldberg, "How graphene slides: Measurement and theory of strain-dependent frictional forces between graphene and SiO2," *Nano Letters*, vol. 13, pp. 2605–2610, 2013.

[3] O. L. Blakslee, D. G. Proctor, E. J. Seldin, G. B. Spence, and T. Weng, "Elastic Constants of Compression-Annealed Pyrolytic Graphite," *Journal of Applied Physics*, vol. 41, no. 8, pp. 3373–3382, 1970.

[4] I. Calizo, A. A. Balandin, W. Bao, F. Miao, and C. N. Lau, "Temperature dependence of the raman spectra of graphene and graphene multilayers," *Nano Letters*, vol. 7, no. 9, pp. 2645–2649, 2007.

[5] J. J. Brown, M. Muoth, C. Hierold, and V. M. Bright, "Electron Diffraction of an In Situ Strained Double-Walled Carbon Nanotube," *Advanced Materials*, vol. 27, no. 4, pp. 766–770. [Online]. Available: https://onlinelibrary.wiley.com/doi/abs/10.1002/adma.201404391